Supporting Information for

Controllable Growth of Vertical Heterostructure $GaTe_xSe_{1-x}$/Si by Molecular Beam Epitaxy

Shanshan Liu,[1] Xiang Yuan,[1] Peng Wang,[2] Zhi-Gang Chen,[3] Lei Tang,[1] Enze Zhang,[1] Cheng Zhang,[1] Yanwen Liu,[1] Weiyi Wang,[1] Cong Liu,[2] Chen Chen,[1] Jin Zou,[3] Weida Hu,[2] Faxian Xiu[1*]*

[1] State Key Laboratory of Surface Physics and Department of Physics, Fudan University, Shanghai 200433, China; Collaborative Innovation Center of Advanced Microstructures, Fudan University, Shanghai 200433, China

[2] National Laboratory for Infrared Physics, Shanghai Institute of Technical Physics, Chinese Academy of Sciences, Shanghai 200083, China

[3] Materials Engineering, The University of Queensland, Brisbane QLD 4072, Australia

[*]Correspondence and requests for materials should be addressed to F. X. (E-mail: faxian@fudan.edu.cn) and W. H. (E-mail: wdhu@mail.sitp.ac.cn)

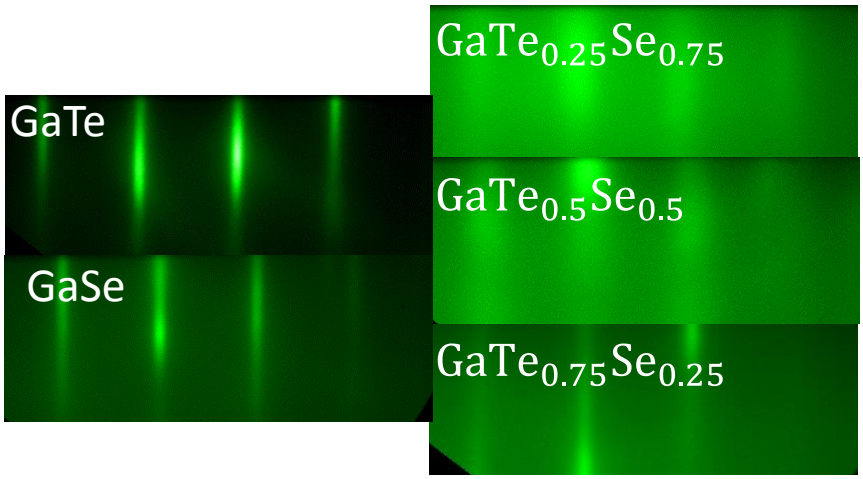

Figure S1. RHEED patterns of $GaTe_xSe_{1-x}$ with different Te composition. We can see that the diffraction patterns of the pure GaTe or GaSe thin films are streaky, while the patterns of alloys become blurry.

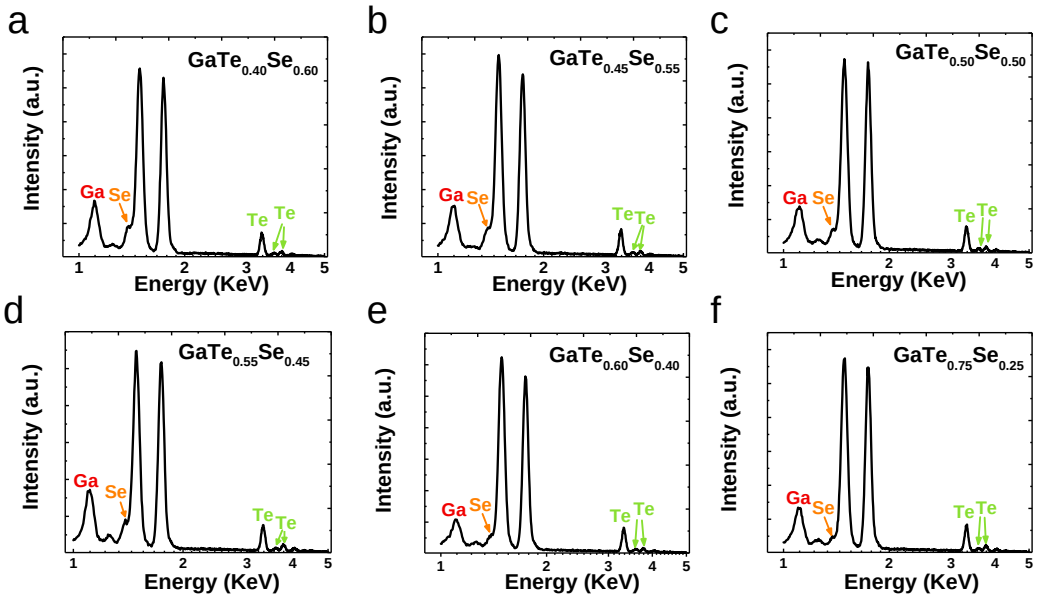

Figure S2. Energy-dispersive X-ray spectra (EDX) of different Te composition.

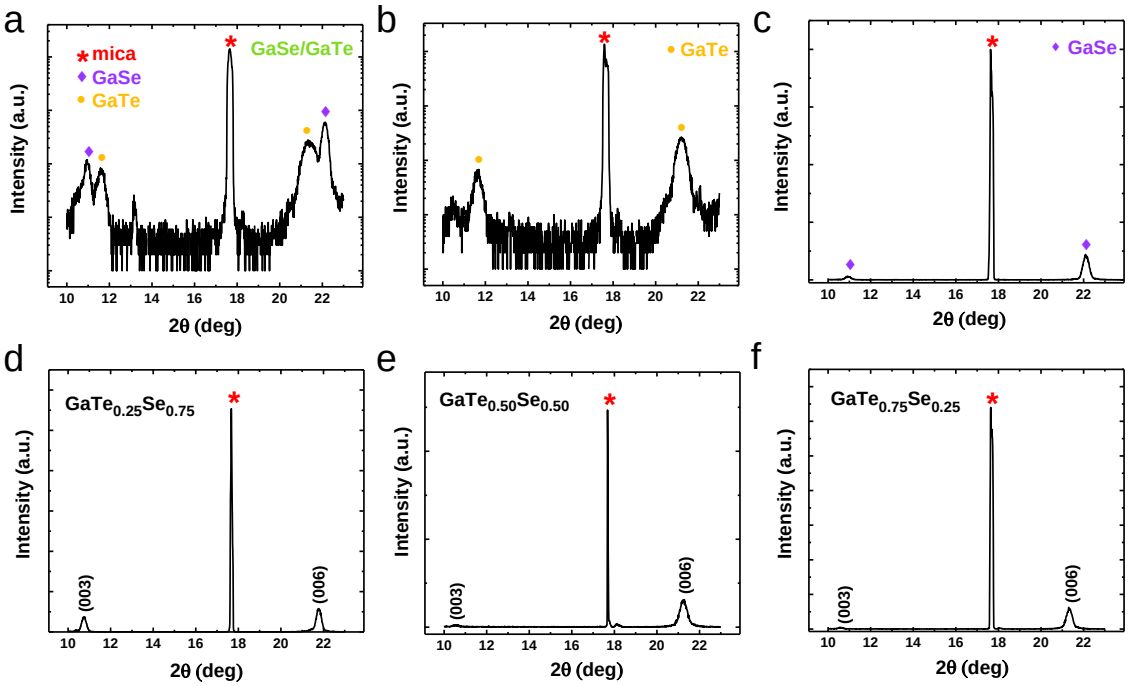

Figure S3. X-ray diffraction spectra of GaSe/GaTe, GaSe, GaTe and GaTeSe thin films. The star"*" marked peak is from mica substrate.

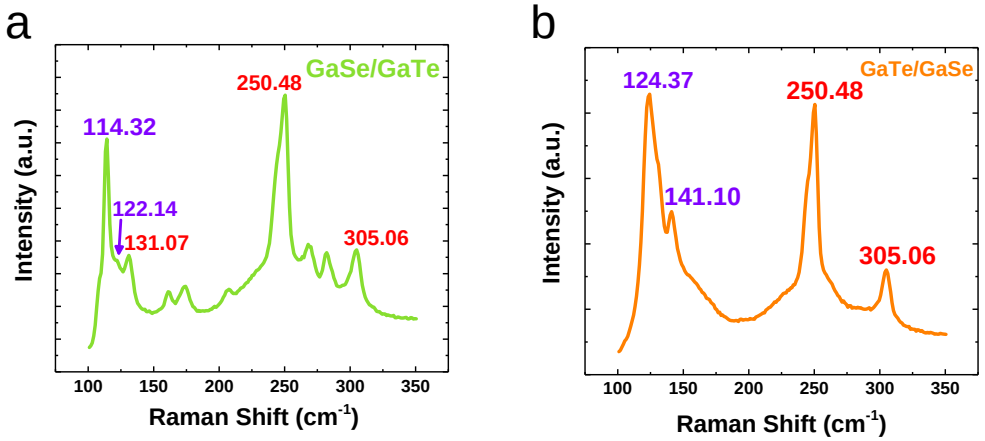

Figure S4. Raman spectra of (a) GaTe/GaSe and (b) GaSe/GaTe heterostructures. The peaks signed with purple originate from GaTe while the red signed are from GaSe. The Raman characteristic peaks consist of peaks from GaTe and GaSe, which are totally different from the Raman frequency of the $GaTe_xSe_{1-x}$ alloys.

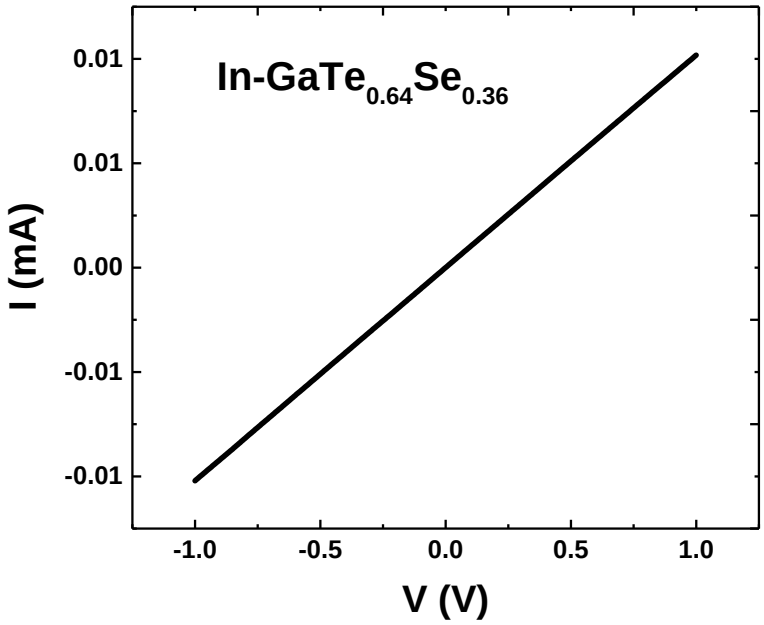

Figure S5. Ohmic contact between In and $GaTe_{0.64}Se_{0.36}$.

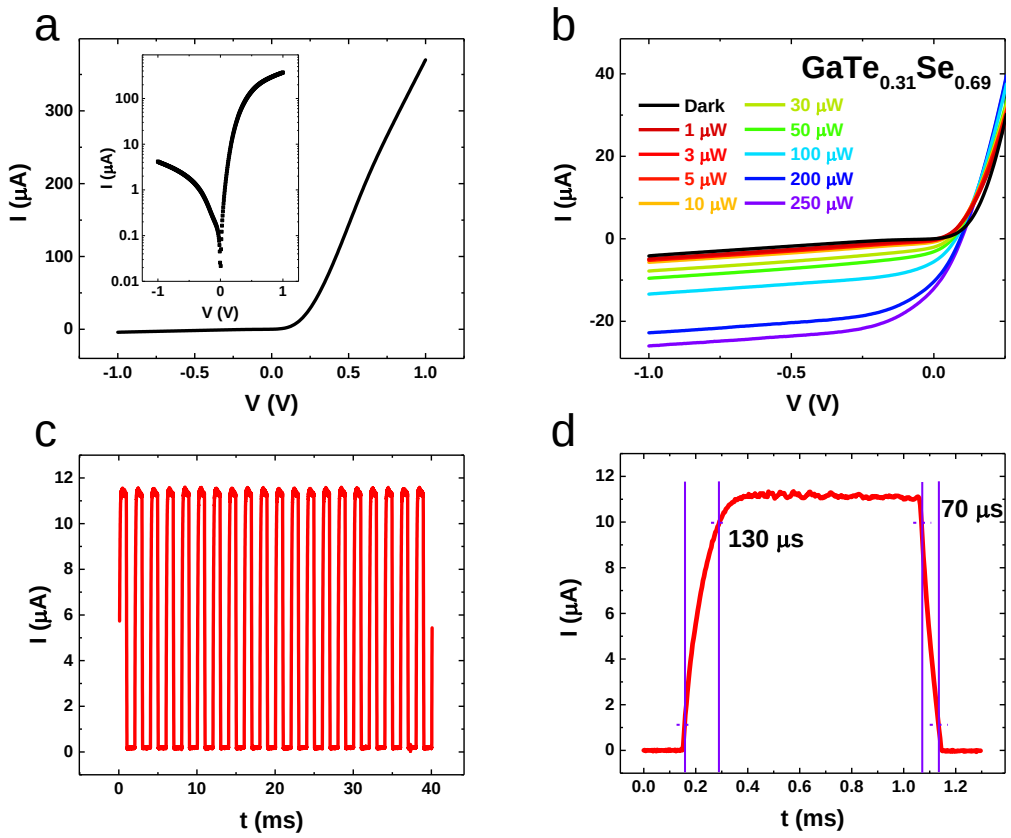

Figure S6. Electrical and optoelectrical measurements of *p-n* junction $GaTe_{0.31}Se_{0.69}$/Si. (a) *I-V* characteristics, the inset is the absolute value of current under different bias, clearly showing the rectifying ratio of 97. (b) *I-V* curves under different laser incident as a function of bias. The behavior is similar to the $GaTe_{0.64}Se_{0.36}$/Si heterostructure described in the main text. (c) Zero-biased photocurrent under circulations of laser on and off, the incident power is 250 μW. The photodiode is robust under millions of operation cycles, and the response does not show any fading behavior. (d) Time-resolved photoresponse. Photoresponse time is defined as the experienced time from the 10 % to 90 % of the maximum photocurrent. It is 130 μs and 70 μs for increasing and falling edges, extremely sensitive when compared to some other photodiodes.

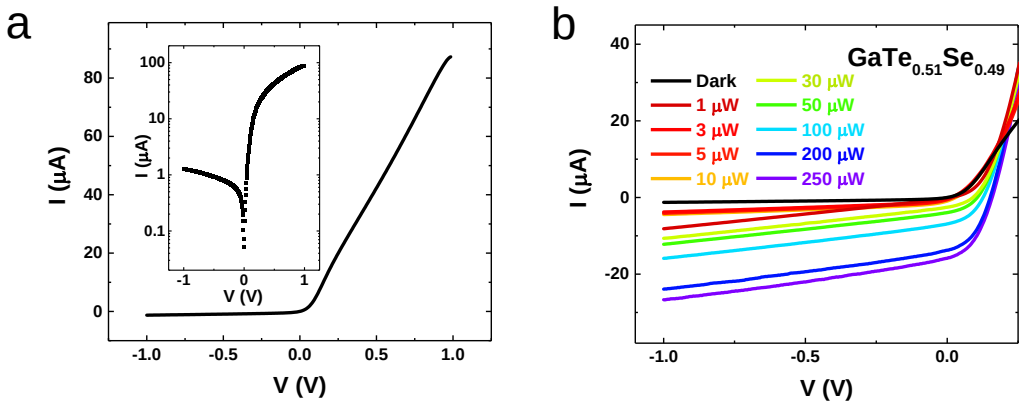

Figure S7. (a) Dark current and (b) *I-V* curves with different laser power levels for a $GaTe_{0.51}Se_{0.49}$/Si diode under different biased voltage. Figure S7a inset is the absolute value of current under different bias with a rectifying ratio of 70.

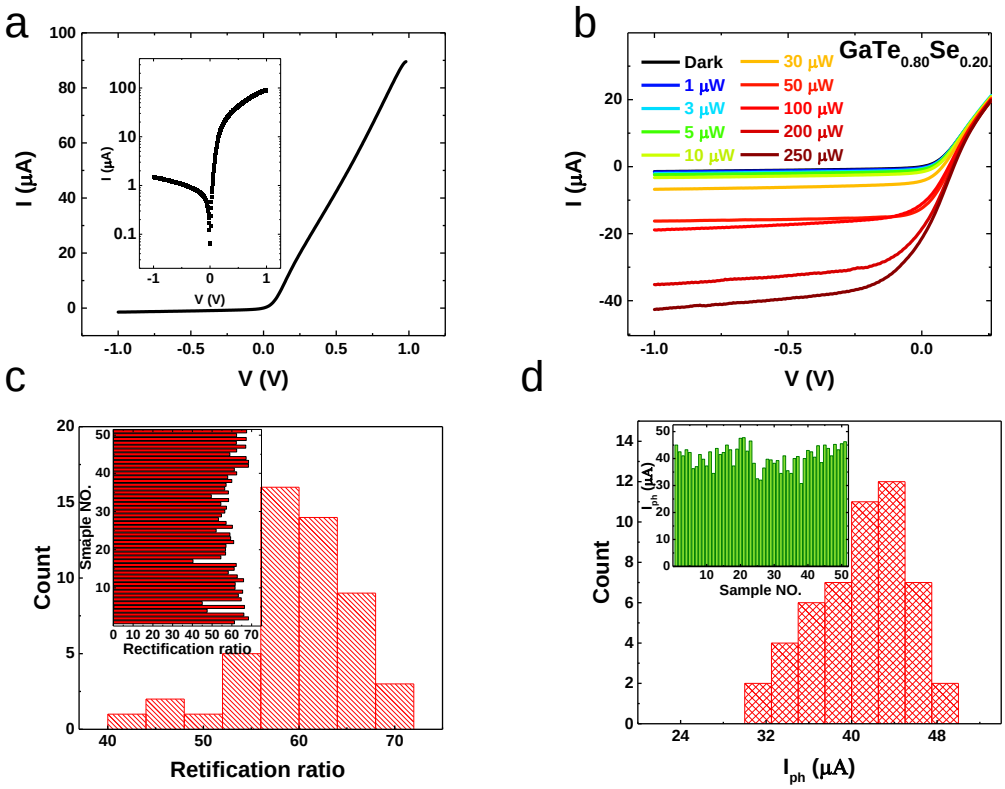

Figure S8. (a) Dark current and (b) *I-V* curves with different laser power levels for a $GaTe_{0.80}Se_{0.20}$/Si diode as the function of different biased voltage. Figure c inset is the absolute value of current under different biased voltage with a rectifying ratio of 60. Distribution of (c) rectifying characteristics and (d) photocurrent under 250 μW incident illumination power. The insets are rectification ratio and photocurrent of each photodiode, respectively.